J Seismol (2013) 17:147–163
DOI 10.1007/s10950-012-9305-8

ORIGINAL ARTICLE

Discrimination of induced seismicity by full moment tensor inversion and decomposition

Simone Cesca · Alexander Rohr · Torsten Dahm

Received: 24 June 2011 / Accepted: 27 April 2012 / Published online: 22 May 2012
© Springer Science+Business Media B.V. 2012

Abstract Human activities, including operations related to mining and reservoir exploitation, may induce seismicity and pose a risk for population and infrastructures. While different observations are commonly used to assess the origin of earthquakes, there is a lack of rules and methods for the discrimination between natural and induced seismicity. The inversion and decomposition of the full moment tensor and the observation of relevant deviation from a pure double couple (DC) model may be an indicator for induced seismicity. We establish here a common procedure to analyse a set of natural and induced events of similar magnitude, which occurred in Germany and neighbouring regions. The procedure is based on an inversion method and on a consistent velocity model and recording network. Induced seismicity is recorded during different mining and/or reservoir exploitations. Moment tensors are inverted using a multi-step inversion approach. This method, which was successfully applied in previous studies at regional and teleseismic distances, is further developed here to account for full moment tensor analysis. We first find a best DC solution and then perform a full moment tensor inversion, fitting full waveforms amplitude spectra at regional distances. The moment tensor solution is decomposed into DC, compensated linear vector dipole and isotropic terms. The discrimination problem is then investigated through the evaluation of distributions of non-DC source components for natural and induced data sets. Results illustrate the potential of the inversion and discrimination approach. Additional detailed analyses are carried out for the two most significant induced earthquakes, and rupture models are compared with the full moment tensor solutions.

Keywords Induced seismicity · Earthquake source · Moment tensor inversion · Isotropic component · Mining seismicity

S. Cesca (✉) · A. Rohr · T. Dahm
Institut für Geophysik, Universität Hamburg,
Bundesstrasse 55,
20146 Hamburg, Germany
e-mail: simone.cesca@zmaw.de

1 Introduction

Induced seismicity may span in size and magnitude from microseismicity recorded at local scale and caused by a variety of human activities and natural transients to large earthquakes induced, for example, by magma and dike intrusions in volcanic regions. A case of significant induced seismicity is given by the Gazli earthquakes (Simpson and Leith 1985). Although the difference between natural, induced and triggered seismicity is well defined, it remains rather difficult to assess, and no common procedures have been established so far. In this work, we limit our application to the comparison of tectonic earthquakes and induced seismicity in mining environments and reservoir exploitation and to the discrimination problem

based on the earthquake source parameters. We follow a pure seismological approach by modelling broadband seismic data at regional distances to derive the point source radiation pattern. In mining and gas/oil extraction environments, different types of mechanisms have been observed and modelled in the past. These may include collapses, rock falls, pillar bursts, explosions, as well as shear cracks. Events induced by reservoir exploitation have mostly shown shear crack failures, often associated to slow ruptures and excitation of low frequency signals (e.g. Ottemöller et al. 2005; Dahm et al. 2007; Cesca et al. 2012).

For a significant part of induced seismicity, the rupture dynamics is common to tectonic events, e.g. occurring as shear failure along weakened surfaces or pre-existing fault systems. In such a case, independently on the origin of the stress field or its perturbation, the seismic energy is released by a shear crack, which can be modelled as a pure double couple (DC) source. However, a significant part of induced events are driven, at least partially, by other dynamics. These include, reducing to the models mentioned above, collapses, rock bursts and cavities deformations. In these cases, the point source model which best describes the seismological observations may significantly differ from a pure DC source. Non-DC components, such as a compensated linear vector dipole (CLVD) and isotropic components, may then be detected. Tectonic events, on the contrary, are always expected to have a negligible isotropic component and a low CLVD component (e.g. Julian et al. 1998; Miller et al. 1998), although estimations of this last term may be in some cases large, as a consequence of source and/or wave propagation mismodelling. This last assumption has led to the implementation of moment tensor inversion routines, both at regional and teleseismic distances, which force the isotropic component to be null. Our aim is to adopt a full moment tensor inversion approach for the analysis of a mixed data set, including natural and induced events, and to judge whether the determination of non-DC can be used to assess the induced origin of an earthquake. Given the previous discussion, the determination of large non-DC source components cannot be used to distinguish in a strict sense between induced and natural seismicity but rather provides a strong indicator for an induced event of a certain type (e.g. collapse or rock burst). The deviation from the theoretical pure DC model is investigated to judge whether the event is induced or not. We focus on a regional data set in central Europe because in this area induced seismicity plays a significant role with respect to the overall seismicity. The data set is composed of 30 earthquakes, 6 of them induced, and includes the two largest induced events ever recorded in the region, which took place in 1989 and 1996. Thanks to the similar range of magnitudes (M_L 3.9–5.9) and depths (0–25 km) of the induced and tectonic events, as well as the adoption of a common seismological network to study them, it is possible to make a direct comparison of the characteristics of the derived source models.

2 Moment tensor and non-DC components

The moment tensor representation (Gilbert 1970) has been widely used in seismology to describe the seismic sources, under a point source approximation. Since the surface displacement can be expressed as the convolution of a moment tensor, describing the source radiation pattern, and Green's functions, accounting for wave propagation from source to receiver, this representation results very suitable for inversion purposes, as confirmed by its widespread use to provide focal mechanisms catalogues (e.g. Dziewonski et al. 1981) as well as for specific earthquake studies. The moment tensor is formally described by a symmetric tensor, which has as entries the generalised force couples (Aki and Richards 1980). The moment tensor can be described by the sum of an isotropic term, reproducing the effects of a volume variation at the focal region, and a deviatoric component. The deviatoric part can be further decomposed and several common decompositions are described in Jost and Hermann (1989). Minson and Dreger (2008) correctly extended the approach to seismic sources with significant isotropic components. We adopt here the most widely used decomposition, by means of a DC and a CLVD term. Significant isotropic component have been found for nuclear explosions, mining collapses and earthquake sources in volcanic environments (Minson and Dreger 2008; Dreger et al. 2008; Ford et al. 2009). We investigate here the relevancy of non-DC source components for the case of seismicity induced by human activities. Hasegawa et al. (1989) discussed six possible failure mechanisms accompanying mining activities. In three cases, the source radiation pattern can be represented by a pure

DC: thrust faulting below the mining region, normal faulting at the mining stope face and shallow near horizontal thrust faulting. Three additional mechanisms show a different radiation pattern, for which large non-DC source components are expected: cavity collapse, pillar burst and tensile failure. Šílený and Milev (2008) have further discussed point source radiation patterns for these possible rupture models. According to the classification proposed by Hasegawa et al. (1989), a cavity collapse model would reproduce the effects of a rock fall, driven by gravity, or a more energetic rock burst. In both models, source patterns would include single forces or a vertical positive dipole, producing positive onsets at all azimuths, and a moment tensor combined by a positive isotropic component and a CLVD with vertical symmetry. A pillar burst represents the effect of a pillar failure and the consequent closing of the cavity. It can be modelled by a convergent vertical dipole, obtained by adding the implosive isotropic term and a vertical CLVD, which explains the negative onsets observed for this failure mode. Finally, a tensile failure of the competent cap rock above mining cavities may occur, most likely where the roof subsidence is greatest. In this last case, horizontal dipoles could be used to describe the source radiation patterns. A combination of the proposed mechanisms can likely take place at the same time, which would result in the superposition of different radiation patterns, and thus a superposition of DC, CLVD and isotropic terms.

All inversions methods routinely used to provide moment tensor catalogues at regional and teleseismic distances (e.g. Dziewonski et al. 1981; Pondrelli et al. 2002; Braunmiller et al. 2002) assume no volumetric seismic sources and retrieve five independent moment tensor components, whereas the sixth component is chosen to fulfil the null isotropic condition. The obtained mechanism is then decomposed into DC and CLVD, and a minor deviation from the pure DC model is in some cases interpreted to judge the solution quality. Non-DC component are in this case limited to the CLVD term. CLVD has been observed and deeply studied for several earthquakes (Julian et al. 1998; Miller et al. 1998; and references therein), both as a consequence of real source features (e.g. landslides, volcanic sources, complex shear faulting and tensile faulting) or as artefact due to the inversion approach and data quality, e.g. in case of wave propagation mismodelling or poor azimuthal coverage. Cesca et al. (2006) showed that spurious terms can affect moment tensor solutions at regional distances when computing Green's functions for incorrect velocity models, and when the network geometry leads to large azimuthal gaps. However, these effects are less critical for amplitude spectra moment tensor inversion with respect to the time domain approach. In the case of explosion, volcanic and induced earthquakes, spurious CLVD components may also reflect the improper assumption that isotropic terms are negligible. The statistical analysis of global and regional moment tensor catalogues illustrates the relevancy of non-DC components affecting focal mechanism solutions. The analysis has been carried out here on two different catalogues (Fig. 1): the Global Centroid Moment Tensor (CMT) catalogue (Dziewonski et al. 1981) and the Swiss Eidgenossiche Technische Hochschule (ETH) regional moment tensor catalogue (Braunmiller et al. 2002; Bernardi et al. 2004), which provides several moment tensor for central Europe (Fig. 1 refers to events in the range of 43–55 ° Lat N and 0–30 ° Lon E) and is the most relevant catalogue for the seismicity analysed in this work. We analyse here subsets of the available catalogues, limited to certain time periods, range of magnitudes and epicentral location; the two catalogue subsets contain 19,150 and 154 events, respectively. The choice of these subsets aims at minimising the effects of poorer quality moment tensor inversion for old time spans (smaller networks, poorer azimuthal coverages), epicentral locations (far from the network, poor azimuthal coverage) and extreme small or large magnitudes (poor data quality or finite rupture effects). A similar, general pattern can be observed for both catalogues; although most of solutions show minor CLVD components, the number of events where CLVD is relevant is quite large. For the chosen subsets, 11.4 % of the events from the Global CMT catalogue and 11.7 % of the events from the Swiss regional catalogue have non-DC components larger than 50 %. Note that the percentage of decomposed terms reflect the ratio of seismic energy released by these mechanisms, and the presence of 50 % CLVD component can be well considered as a very large discrepancy from the pure DC model. The average percentage of the non-DC component slightly increases with depth, possibly as a consequence of larger signal-to-noise ratio for seismic waveforms of shallower earthquakes waveforms, where surface waves are more

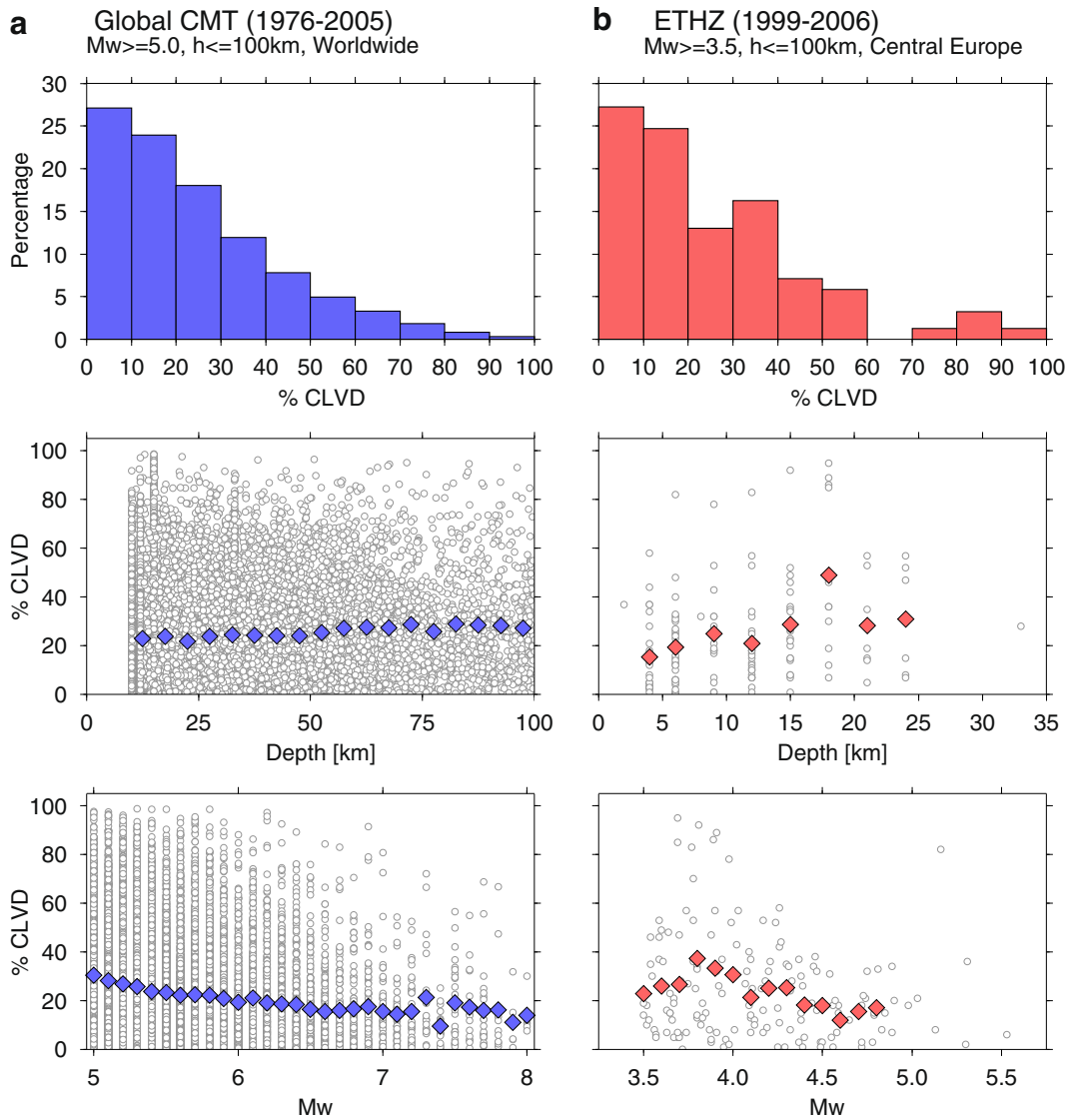

Fig. 1 Statistics of non-DC (*CLVD*) components for the Global CMT catalogue (**a**, *blue*) and the ETH regional catalogue (**b**, *red*). Only subsets of the catalogues are considered, according to the indicated (*top*) magnitude, depth and location ranges. *Top*, histogram representation of the percentage of events with different CLVD percentages. *Centre*, relation between CLVD percentage and source depth (*white circles* denote single events; *diamonds* denote average values per depth interval). *Bottom*, relation between CLVD percentage and moment magnitude (*white circles* denote single events; *diamonds* denote average values per magnitude interval)

excited. A more pronounced variation of the average non-DC term can be observed with respect to magnitudes, with larger events showing, in general, lower non-DC components. This result is not surprising and can be again related to a better data quality for larger events. The different pattern which is seen for events with magnitude below M_L 4.0 in the Swiss regional catalogue has to be related with the preferred location and data quality of the smallest events, which are only analysed in favourable conditions. These results illustrate the need of a careful evaluation of the network performance and inversion stability, when using a moment tensor inversion approach to discriminate between cases where the non-DC represent a real source

feature, from those where it is a spurious term due to limitations of the modelling approach.

3 Full moment tensor inversion methodology

Several codes are available to perform moment tensor inversion, although only part of them can be used to derive a full moment tensor source. Significant applications of full moment tensor inversion techniques to selected case studies have been shown by Dreger et al. (2008) and Ford et al. (2009), using a pure time domain inversion approach. We use here the Kiwi tools (Heimann 2011), to implement a combined inversion approach working in the frequency (fit of amplitude spectra) and time domain (fit of displacement waveforms). The Mopad tool (Krieger and Heimann 2012) is used to perform source decomposition and to plot moment tensor solutions. The moment tensor is first decomposed into isotropic and deviatoric terms; the decomposition of the deviatoric term is not unique (e.g. Vavrycuk 2001) and we follow the standard DC–CLVD decomposition, according to Jost and Hermann (1989). We adopt the general approach of a multi-step inversion scheme (Cesca et al. 2010), extending the method to additionally account for full moment tensor sources. Our approach provides both a DC and full MT solution and evaluates the significance of the fit improvement between the two source models. The chosen data set is characterised by moderate magnitude shallow events. Surface waves are in general well recorded up to 500 km epicentral distance, showing the largest signal-to-noise ratios at frequencies in the range of 0.02–0.10 Hz, while body-waves often show unclear onsets and poor quality. As a consequence, in our approach, we will always fit low frequency (below 0.1 Hz) full waveform data. Data preprocessing include removal of mean and trend, tapering in the time domain and deconvolution of the instrumental response to obtain displacement traces. In the first inversion step, we perform a DC inversion by fitting amplitude spectra of all available displacement components, according to Cesca et al. (2010), and obtain a DC source model (with the intrinsic polarity ambiguity of amplitude spectra inversions), centroid depth and scalar moment. The misfit (M_{DC}) is expressed as L^2 norm between synthetic and observed amplitude spectra. In the next step, we investigate the space of full MT sources. We fit amplitude spectra as in inversion step 1, and iteratively perform a set of Levenberg–Marquardt inversions for a grid of starting solutions. These include the best DC source from inversion step 1, a pure isotropic source, as well as CLVDs and tensile cracks with different orientations. A second L^2 norm misfit (M_{MT}) is then retrieved for the best fitting full MT source, which is then decomposed into DC, CLVD and isotropic component. The new misfit estimation is always smaller than or equal to M_{DC}, since the space of DC sources is a subspace of the space of full moment tensors; the number of source parameters raise from 4 to 6, passing from the DC to the full MT inversion. The significance of misfit improvement from M_{DC} to M_{MT} is assessed using the Bayesian Information Criterion (BIC, Kass and Raftery 1995). The BIC values are computed for both modelling approaches following the equation:

$$\mathrm{BIC} = k \ln(n) + n \ln(R/n) \tag{1}$$

where k is the number of free parameters plus 1, n is the number of data points (here frequency samples for all amplitude spectra) and R is the misfit. The lowest BIC value indicates the preferred model, penalising models with larger number of free parameters. In the third inversion step, the two possible polarities of the best full MT focal mechanism are tested, by fitting shifted seismograms in the time domain (the maximal accepted shift is ±2 s).

Source parameters uncertainties are relevant for a safe interpretation of results and are here assessed using a jackknife approach. The inversion is repeated 50 times, each time randomly removing 10 % of the available data traces. The estimated parameters, including scalar moment, depth, fault plane angles and percentages of decomposed moment tensor terms, are analysed statistically. In particular, we discuss the variability of the non-DC component of the source, which is here defined as the sum of CLVD and ISO percentages. For pure shear sources, we expect a distribution of estimated non-DC with a maximum close to 0 and a tail towards positive values (by definition, the non-DC parameter cannot have negative values); for a closing crack, we expect a significant non-DC term. A normal distribution could be used in the second case but would overestimate the average and standard deviation for pure shear crack sources. In order to have a common approach, we describe the non-DC distributions using weighted average and standard deviation. The weight of each non-DC estimation

is given by the number of solutions falling within ±5 % of non-DC. Uncertainties can then be estimated, e.g. for a confidence interval of 90 %.

The focal discrimination problem can be also solved by estimating the probability that an event pertains to a certain class of sources, e.g. shear crack (DC) or collapse (C) events, following a Bayesian approach. This approach has been successfully used by Passarelli et al. (2011; this issue) to discriminate between dike-triggered- and tectonic earthquakes. Given the two possible scenarios (DC, C), we apply the Bayes theorem and derive the following posterior probabilities:

$$p(\mathrm{DC}|\mathrm{E}) = \frac{p(\mathrm{DC})p(\mathrm{E}|\mathrm{DC})}{p(\mathrm{DC})p(\mathrm{E}|\mathrm{DC}) + p(\mathrm{C})p(\mathrm{E}|\mathrm{C})} \quad (2a)$$

$$p(\mathrm{C}|\mathrm{E}) = \frac{p(\mathrm{C})p(\mathrm{E}|\mathrm{C})}{p(\mathrm{DC})p(\mathrm{E}|\mathrm{DC}) + p(\mathrm{C})p(\mathrm{E}|\mathrm{C})} \quad (2b)$$

The posterior probability $p(\mathrm{DC} \mid \mathrm{E})$ and $p(\mathrm{C} \mid \mathrm{E})$ for the two scenarios depend on the prior probability ($p(\mathrm{DC})$, $p(\mathrm{C})$) and the likelihoods of the earthquake for these scenarios ($p(\mathrm{E} \mid \mathrm{DC})$, $p(\mathrm{E} \mid \mathrm{C})$). The prior probability indicates the likelihood of the given scenario, based on information complementary to the inversion results; in the following, we will assume a non-informative a priori probability for each scenario (both cases are equally likely to occur a priori). A data set of full MT focal mechanisms could be used in the future to define prior probabilities, based on the percentages of DC and collapse type events which have occurred in a given epicentral region. Another example of prior could be, in the case mining blasts are analysed instead of collapses, the timing of the events according to the mining procedures.

The likelihood of the earthquake for the chosen scenario can be obtained from the source parameters derived by the moment tensor inversion. Since our study focuses on the moment tensor decomposition to perform the discrimination, the chosen parameters should reflect the percentages and signs of the moment tensor decomposed terms. To this goal, we will adopt a source type representation (Hudson et al. 1989), where moment tensors are plotted in two-dimension diagrams; the parameter on the horizontal scale describes the type of constant volume component in the source (DC vs. CLVD), while the parameter on the vertical scale describes the proportion of the volumetric change component. The probability of occurrence (likelihood) of the earthquake for both scenarios ($p(\mathrm{E} \mid \mathrm{DC})$ and $p(\mathrm{E} \mid \mathrm{C})$) are obtained using the following equations:

$$P(\mathrm{E}|\mathrm{DC}) = P(\mathrm{E})P(\mathrm{DC}) \quad (3a)$$

$$P(\mathrm{E}|\mathrm{C}) = P(\mathrm{E})P(\mathrm{C}) \quad (3b)$$

where $P(\mathrm{E})$ is the probability density function derived from the range of moment tensor solutions (following the jackknife approach), and $P(\mathrm{DC})$ and $P(\mathrm{C})$ are expected probabilities defined for the natural and induced seismicity moment tensors, independent from the inversion algorithm, which will be discussed in the following sections.

4 German data set, tectonic and induced seismicity

Natural and man-induced seismicity are analysed here for the case of Germany and neighbouring regions. Induced seismicity has a major importance in Germany and central Europe (Fig. 2), both owing to moderate natural seismicity and to relevant mining activities. According to our investigation, based on the recompilation of regional catalogues (Bundesanstalt für Geowissenschaften und Rohstoffe (BGR), ETH, KNMI), approximately 12 % of all earthquakes with local magnitude from 3 to 5 are caused by human activity of different types. This percentage is even higher (24 %), when considering events with local magnitudes above 4.5. The largest tectonic and induced events which occurred in this region in the last 25 years were the 13 April 1992 Roermond (M_L 5.9) and the 13 March 1989 Völkershausen event (M_L 5.6), respectively. Comparable maximal magnitudes indicate that natural and induced seismicities pose similar hazards and may produce similar damages in this region. The event data set has been chosen by limiting the epicentres to a region defined by 46–56 ° latitude north and 5–15 ° longitude east and the time frame to the period of 1989–2011. All events with magnitudes above M_L 4.0 from the last 10 years, plus larger or significant events since 1989, have been included in our data set. The resulting data set is composed by 24 natural and 6 induced events (Fig. 3). Induced seismicity has been related to coal mining (Ibbenbüren, 6

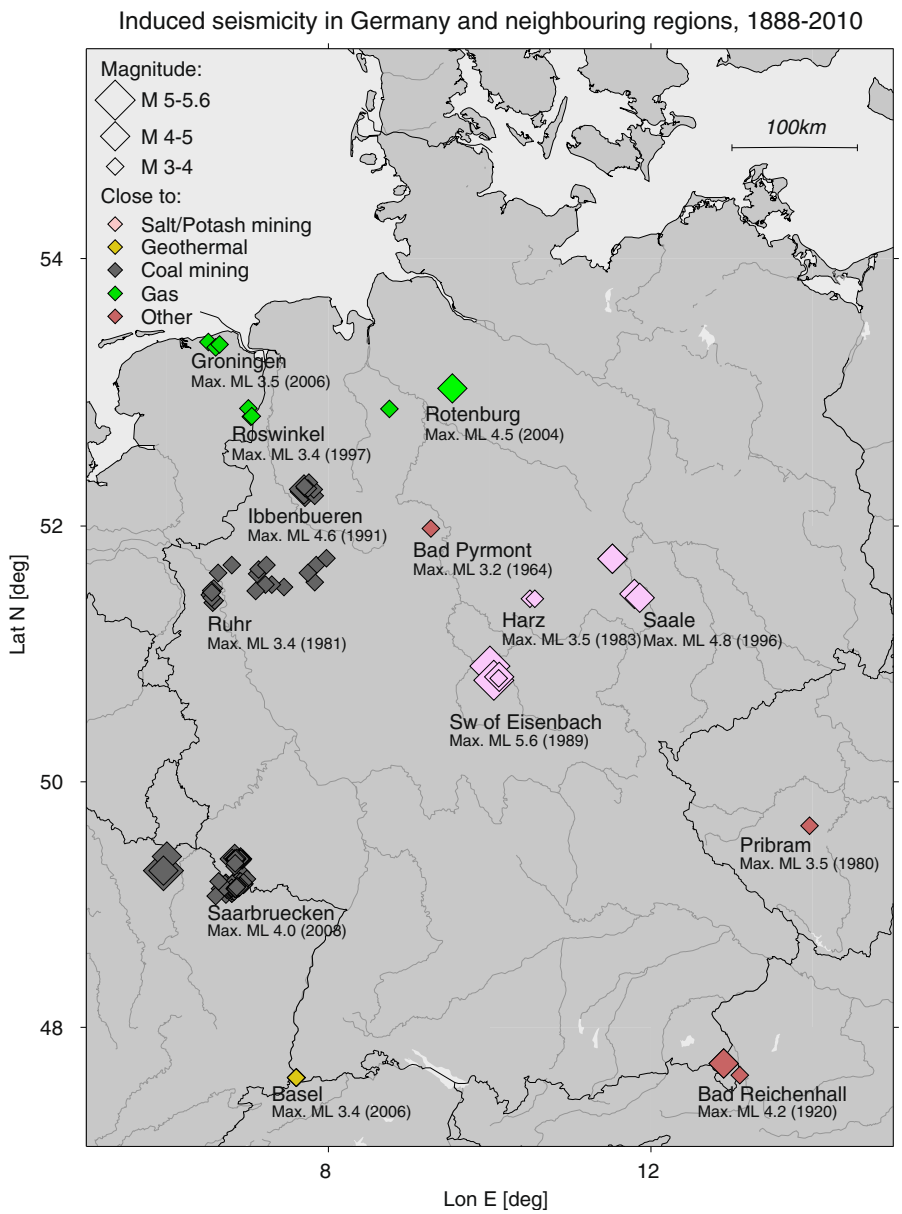

Fig. 2 Induced seismicity in Germany and neighbouring regions since 1888. *Diamonds of different colours* (see legend, *top left*) denote induced seismicity of different types. Symbol size scale with magnitudes (ML scale, according to BGR catalogue)

January 2003, M_L 3.9; Saarbrücken, 23 February 2008, M_L 4.0), potash mining (Völkershausen, 13 March 1989, M_L 5.6; Teutschenthal, 11 September 1996, M_L 4.8) and gas field exploitation (Rotenburg, 20 October 2004, M_L 4.5; Syke, 15 July 2005, M_L 3.8). Natural and induced seismicity data sets present similar magnitudes and epicentral locations. Although all chosen events are shallow (crustal) earthquakes, the induced seismicity data set is shallower than the natural data set. We choose here a common inversion framework. Source inversions are performed using data from a common station configuration (Fig. 3) composed by broadband seismometers from regional networks (German Regional Seismic Network—GRSN, Swiss Seismological Network, Czech Seismic Network, Austrian Seismic Network), as well as few broadband stations from GEOFON, GEOSCOPE and MEDNET networks. The inclusion of stations from neighbouring countries allows similar stations distributions and azimuthal coverages for earthquakes which are located at the edges of the study regions. Green's functions have been computed using QSEIS

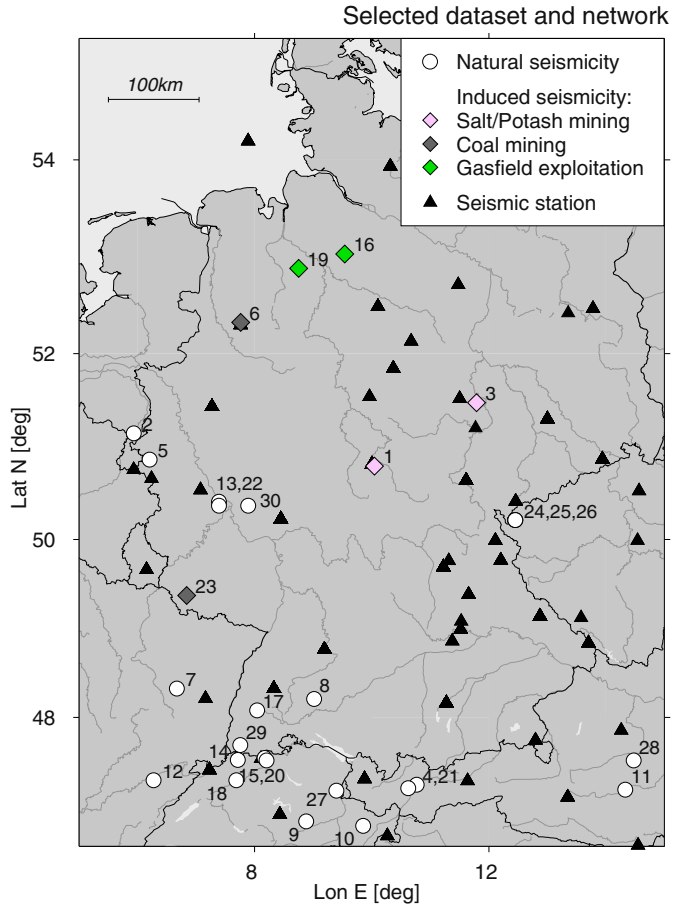

Event	Day	M
1. Volkerhausen	13.03.1989	5.6
2. Roermond_NL	13.04.1992	5.9
3. Teutschenthal	11.09.1996	4.8
4. Imst_A	05.06.1997	4.4
5. S_Kerkrade	22.07.2002	4.9
6. Ibbenbueren	06.01.2003	3.9
7. Vosgian_mts	22.02.2003	5.9
8. Swaebian_Jura	22.03.2003	4.4
9. Linthal_CH	06.05.2003	4.4
10. Scalettapass_CH	18.07.2003	3.9
11. Murau_A	21.07.2003	4.4
12. Besancon_F	23.02.2004	5.5
13. Koblenz	22.05.2004	3.7
14. Saeckingen	21.06.2004	4.1
15. Laufenburg	28.06.2004	4.2
16. Rotenburg	20.10.2004	4.5
17. Waldkirch	05.12.2004	5.4
18. Olten_CH	12.05.2005	4.1
19. Syke_Bremen	15.07.2005	3.8
20. Laufenburg	12.11.2005	4.1
21. Landeck_A	19.05.2007	4.2
22. Koblenz	03.08.2007	3.9
23. Saarbruecken	23.02.2008	4.0
24. Erzgebirge	10.10.2008	4.2
25. Erzgebirge	14.10.2008	4.0
26. Erzgebirge	28.10.2008	4.1
27. Vaduz_FL	04.01.2009	4.4
28. Admont_A	20.04.2009	4.2
29. Schopfheim	05.05.2009	4.5
30. Koblenz	14.02.2011	4.5

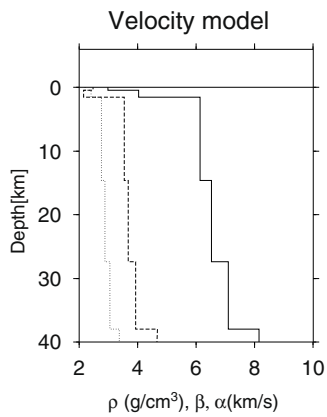

List of stations

Name.Nw	Lat N	Lon E	Name.Nw	Lat N	Lon E	Name.Nw	Lat N	Lon E
UBBA.GR	50.819	10.001	ROTZ.BW	49.767	12.207	DREG.GR	50.663	6.233
NRDL.GR	52.494	10.107	TANN.SX	50.415	12.462	BNI.MN	45.052	6.678
FUORN.CH	46.620	10.263	RJOB.GR	47.737	12.796	AHRW.GR	50.541	7.076
BSEG.GR	53.935	10.317	WET.GR	49.144	12.878	ECH.G	48.216	7.159
CLZ.GR	51.842	10.372	CLL.GR	51.308	13.003	BOURR.CH	47.394	7.230
ASSE.GR	52.130	10.673	RGN.GR	54.548	13.321	BUG.GR	51.441	7.269
GRA1.GR	49.692	11.222	KBA.OE	47.078	13.345	SENIN.CH	46.363	7.299
GRFO.GR	49.691	11.220	BRNL.GR	52.428	13.358	IBBN.GE	52.306	7.759
FUR.GR	48.163	11.275	KHC.CZ	49.131	13.578	HLG.GE	54.185	7.884
GRA3.GR	49.762	11.319	GEC2.GR	48.845	13.702	SULZ.CH	47.528	8.112
GRC2.GR	48.868	11.376	RUE.GR	52.476	13.780	BFO.GR	48.330	8.330
T9BG.TO	52.723	11.479	BRG.GR	50.873	13.943	BNALP.CH	46.871	8.425
WIMM.SX	51.521	11.505	MOA.OE	47.849	14.266	TNS.GR	50.222	8.447
GRC1.GR	48.996	11.521	PRU.CZ	49.988	14.542	FUSIO.CH	46.455	8.663
GRC4.GR	49.087	11.526	OBKA.OE	46.509	14.549	STU.GE	48.771	9.194
MOX.GR	50.645	11.616	PVCC.CZ	50.528	14.569	TUE.MN	46.472	9.347
WTTA.OE	47.264	11.636	ARSA.OE	47.251	15.523	DAVA.OE	47.287	9.880
GRB1.GR	49.391	11.652	SSB.G	45.279	4.541	GTTG.GR	51.545	9.965
NEUB.SX	51.208	11.775	HGN.GR	50.764	5.932			
MANZ.BW	49.986	12.108	WLF.GE	49.665	6.153			

Fig. 3 Selected data set and network configuration. Natural (*circles*) and induced (*diamond*) events are plotted using *different colours*, according to the legend. *Black triangles* denote stations used in this study (few stations are out of the map, but a full list is given in the bottom of the figure). Event names, days of the occurrence and magnitude estimations (ML scale, according to BGR catalogue) are listed. The adopted velocity model is shown at the *bottom left* (*dotted*, *dashed* and *thin lines* denote density, S wave and P wave depth profiles, respectively)

code (Wang 1999) for three different regional velocity models. After preliminary tests (Rohr 2011), we chose the velocity model shown in Fig. 3, which is consistent with the one adopted by Cesca et al. (2010) for the

same region. Moment tensor results with other models are similar but show worse amplitude spectra and waveforms fits. ETH and MEDNET catalogues provide moment tensor solutions, with a null isotropic component constraint, for some of the events here studied. Cesca et al. (2010) also include some reference double couple solutions for a part of these events. The availability of reference focal mechanisms is useful to control the consistency of our results, although no information is available on the isotropic component. Finally, specific studies concerning observations and modelling for the most significant natural and induced events (Krüger and Klinge 2002; Teyssoneyre et al. 2002; Dahm et al. 2007; Braunmiller et al. 2007; Fischer et al. 2010) are also available. Our results will be discussed and compared with previous findings, and proposed source models will be analysed for consistency with different available geophysical observations.

5 Discrimination of natural and induced seismicity

The best double couple and full moment tensor solutions are listed in Fig. 4, where focal spheres are also plotted and compared with other available solutions (Bernardi et al. 2004; Pondrelli et al. 2004, 2007; Dahm et al. 2007; Braunmiller et al. 2007; Fischer et al. 2010; Deichmann 2011). Focal mechanisms and scalar moments are in good agreement with prior solutions, although these are only available for natural earthquakes, with the exception of the 20 October 2004 Rotenburg earthquake, where a rupture close to a DC model is also commonly proposed. The performance of the DC inversion method for natural events was assessed through several previous successful applications (Cesca et al. 2010; Buforn et al. 2011; Custodio et al. 2012). Magnitudes estimated for the natural (M_w 3.3–4.7) and induced (M_w 3.6–4.9) data sets are comparable. It is worth to note that induced seismicity hypocentres cluster at shallower depths, and that no induced earthquake considered here has a centroid depth larger than 10 km. Natural events span over a larger range of depths within the crust. This finding suggests that a combined analysis of source component patterns and source depth could be used for discrimination purposes.

Double couple and full moment tensor solutions are obtained for all events, and misfits are estimated in both cases. According to the methodological discussion, the misfit obtained by fitting data with a MT model always improves (can be theoretically equal or larger) the misfit obtained by assuming the best DC model. We introduce here the misfit improvement, defined as the relative improvement of the misfit when passing from the DC to the MT model. A small misfit improvement either indicates that the preferred MT solution is very close to a DC solution or that the focal mechanism solution is not well constrained and different DC or non-DC solutions can fit the data similarly well. In such case, even in presence of large non-DC estimations, the source model should not be used to discriminate an induced event, as the full moment tensor solution has limited reliability. The significance of the misfit improvement is assessed using the BIC (see Eq. 1). Only events which show a relevant non-DC term and a preferred MT solution are safe candidates for induced seismicity dominated by non-DC failure modes. The overview of DC and non-DC components for all studied events is shown in Fig. 5, both for single events and with respect to depths and magnitudes; events where the full MT is preferred based on BIC are highlighted by blue circles.

Non-DC components for tectonic events in our data set are always below 38 %, with an average percentage of 22 %. This value is comparable with the percentage of 25 %, which is obtained by averaging CLVD percentages for a subset of the ETH regional moment tensor catalogue (see Fig. 1). Few natural events show large misfit improvement, but they are never associated to significant non-DC components; thus, they cannot be misinterpreted as possible candidates of induced seismic events. Our analysis suggests a time evolution of the non-DC components estimations for natural earthquakes (events are ordered chronologically in Fig. 5 left), which has to be related with network improvements since 1989. A similar pattern has also been identified for a global catalogue, by analysing the time evolution of average (yearly) CLVD terms for the Global CMT catalogue.

Induced seismicity considered in this study shows a very variable behaviour. Although the number of discussed events is relatively small, some major considerations can still be made first: potash mining- and coal mining-induced events show non-DC components (39–65 %) larger than the average for natural seismicity, whereas seismicity observed nearby gas fields or directly related to gas exploitation do not show any source mechanism anomaly (non-DC components 14–19 %). The oldest and largest induced

Id	Event	Mw	Depth	DC/ISO/CLVD	Mxx	Myy	Mzz	Mxy	Mxz	Myz	M_0 (Nm)
1	Volkerhausen	4.9	1.0	48 / 34 / 18	0.64	0.59	0.26	-0.05	-0.11	0.86	4.14E+16
2	Roermond_NL	5.3	13.0	68 / 2 / 30	0.69	0.68	0.24	-0.07	-0.15	0.86	1.27E+17
3	Teutschenthal	4.5	1.0	35 / 23 / 42	0.06	0.27	-0.18	0.49	-0.14	-0.83	9.86E+15
4	Imst_A	3.9	18.0	62 / 20 / 18	-0.6	-0.7	0.5	0.15	0.09	-0.1	1.03E+15
5	S_Kerkrade	4.5	14.0	81 / 7 / 12	-0.24	-0.28	-0.15	0.97	-0.24	0.07	9.66E+15
6	Ibbenbueren	3.6	3.0	61 / 20 / 19	0.58	0.34	-0.7	0.57	0.11	-0.53	4.72E+14
7	Vosgian_mts	4.7	10.6	84 / 12 / 4	-0.4	-0.01	1.85	0.44	-0.92	0.47	1.96E+16
8	Swaebian_Jura	4.0	15.7	63 / 3 / 34	0.01	0.55	-0.89	0.56	0.31	-0.18	1.79E+15
9	Linthal_CH	3.6	3.3	75 / 5 / 20	-0.39	0.73	0.38	0.78	-0.08	-0.25	4.72E+14
10	Scalettapass_CH	3.5	12.9	75 / 8 / 17	0.59	-0.35	0.05	0.75	0.15	0.24	2.74E+14
11	Murau_A	3.9	12.0	73 / 25 / 2	-0.61	0.35	0.4	0.5	0.06	0.52	1.38E+15
12	Besancon_F	4.4	15.2	70 / 19 / 11	-0.25	0.76	0.57	-0.49	0.24	0.63	5.82E+15
13	Koblenz	3.6	17.1	85 / 7 / 8	0.4	-0.91	-0.73	0.13	0.46	0.51	3.76E+14
14	Saeckingen	3.3	24.3	74 / 8 / 18	0.79	-1.09	-0.09	0.28	-0.26	-0.05	1.37E+14
15	Laufenburg	3.5	24.6	70 / 19 / 11	0.05	0.96	-0.47	0.55	0.54	-0.36	2.73E+14
16	Rotenburg	4.4	6.2	86 / 7 / 7	-0.12	0.5	-0.58	0.42	0.9	0.39	6.73E+15
17	Waldkirch	4.5	12.1	93 / 6 / 1	-0.4	0.9	-0.65	0.0	0.47	0.33	9.29E+15
18	Olten_CH	3.6	24.4	82 / 5 / 13	-0.4	0.45	-0.35	0.8	-0.41	0.26	3.6E+14
19	Syke_Bremen	3.6	4.8	81 / 0 / 19	-0.87	0.32	0.34	0.52	0.22	0.52	4.86E+14
20	Laufenburg	3.7	20.0	97 / 2 / 1	-0.71	0.54	0.7	0.29	0.53	0.53	5.09E+14
21	Landeck_A	3.6	22.0	72 / 25 / 3	0.32	0.73	-1.05	0.59	0.37	-0.2	4.5E+14
22	Koblenz	3.8	23.0	71 / 14 / 15	0.03	-0.05	-0.07	0.65	0.35	-0.2	9.37E+14
23	Saarbruecken	4.0	2.0	45 / 13 / 42	0.93	-0.59	-0.17	0.21	0.07	0.41	1.6E+15
24	Erzgebirge	3.8	19.2	82 / 13 / 5	0.51	-0.15	0.31	0.6	0.93	1.78	9.64E+14
25	Erzgebirge	3.5	13.9	89 / 8 / 3	0.44	0.02	-0.47	0.56	0.0	-0.58	3.02E+14
26	Erzgebirge	3.6	13.8	73 / 20 / 7	0.34	-0.25	-0.08	0.87	-0.01	-0.53	4.32E+14
27	Vaduz_FL	3.9	14.7	78 / 19 / 3	0.37	0.6	-0.2	0.72	0.26	-0.52	1.01E+15
28	Admont_A	4.2	16.3	87 / 0 / 13	-0.29	0.6	0.26	0.44	-0.0	0.17	3.7E+15
29	Schopfheim	3.6	9.8	75 / 2 / 23	-0.12	-0.12	0.2	-0.79	0.21	-0.48	3.96E+14
30	Koblenz	4.0	9.6	96 / 0 / 4	-0.61	0.31	0.34	0.81	0.14	0.27	1.83E+15

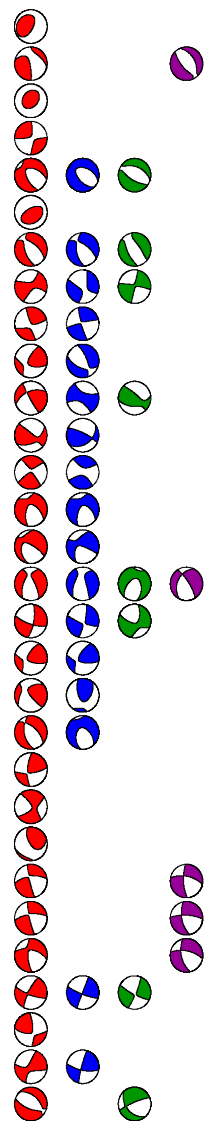

Fig. 4 Overview of moment tensor inversion results. Source parameters are listed for all events in the data set. Focal mechanism solutions (*red*) are compared with available reference solutions: *blue* (ETH catalogue), *green* (MEDNET) and *purple* *focal sphere* (Braunmiller et al. 2007; Dahm et al. 2007, average results for the 2008 seismic swarm in West Bohemia after Fischer et al. 2010)

events in the data set, the Völkershausen (13 March 1989, M_w 4.9) and Teutschenthal (11 September 1996, M_w 4.6) earthquakes show the largest deviations from the pure DC model. The analysis of uncertainties indicates that our approach can be used to discriminate their induced origin. For the Teutschenthal event, the large non-DC term is also accompanied by a clear improvement of amplitude spectra fit when using a full MT model, rather than a pure DC. For the Völkershausen event, the MT is more poorly constrained, as demonstrated by a lower misfit improvement. In this case, however, we are analysing a rather old event (1989), where the number of available stations and their uneven distribution pose strong limitations to waveform inversion. Focal mechanisms are characterised in both cases by large implosive isotropic components and vertical or sub-vertical CLVDs, which are consistent with pillars failure accompanied

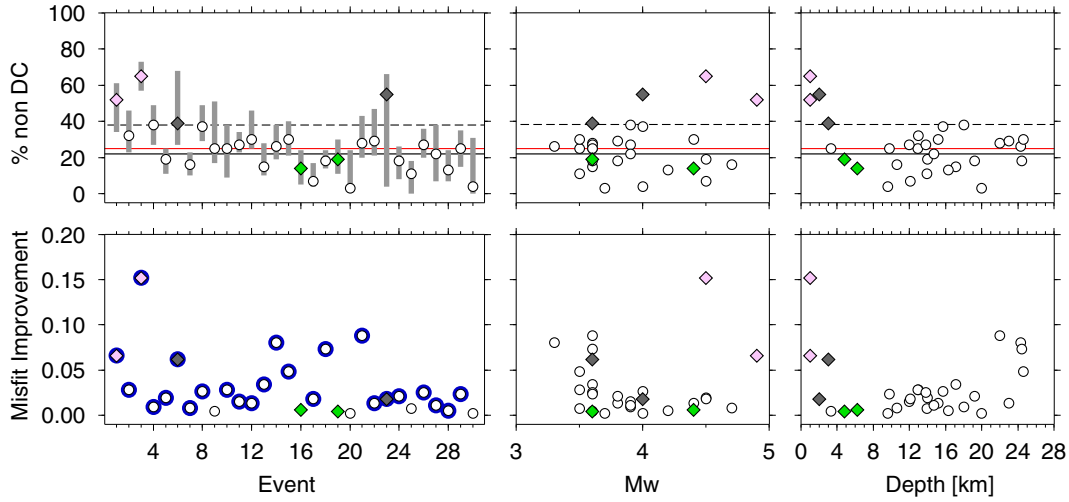

Fig. 5 Non-DC percentage (*top*) and misfit improvement from the DC to the MT solution (*bottom*). Different plots illustrate single event results (*left*), as well as non-DC percentage and misfit improvement variation with respect to magnitude (*centre*) and depth (*right*). Different symbols are used to denote induced (*diamond*) and natural (*circle*) seismicity, according to the legend in Fig. 3. Uncertainties (90 % confidence level) are calculated for induced events using a jackknife approach and shown in the *top left plot* as *grey bars*. A *black line* denotes the average value derived from natural seismicity, a *red line* the average non-DC from a subset of the ETH catalogue (as in Fig. 1) and a *dashed black line* the maximal non-DC from the natural seismicity data set. *Blue circles* in the *lower left plot* denote events for which the full MT solution is preferred to the DC one, based on the Bayesian Information Criterion

by the closing of subsurface mining cavities and roof collapse. The Teutschenthal and Völkershausen events are further discussed in the following chapter, and source models here obtained are further discussed, to judge their fit and consistency with other proposed solutions and with all available geophysical observations. Coal mining-induced events also show significant non-DC components (39–55 %), which may possibly be a real feature of the rupture process. However, in our approach, these source components are not large enough to safely identify them as induced events and to distinguish them with respect to the natural background seismicity (Fig. 5). Finally, seismic events which may be related to gas field exploitation show focal mechanisms which are consistent with a pure DC model. This finding was already outlined by Dahm et al. (2007) for the Rotenburg earthquake.

We follow then the Bayesian approach discussed in the last part of the methodological section. We define two possible expected probabilities p(DC) and P(C) with the aid of source type plots (Hudson et al. 1989). These plots better reflect the moment tensor decomposition: pure DC sources are plotted at the centre, explosive and implosive sources at the top and bottom, and positive and negative CLVDs at the left and right sides. We define expected probabilities (Fig. 6) for the case of pure DC and collapse sources. In the first case (Fig. 6a), the maximal probability is expected at the centre of the plot and decay faster in presence of isotropic terms rather than for CLVD terms (the probability decay for CLVD terms has been chosen consistently to CLVD percentages in the ETH catalogue). In the case of collapse sources, the prior probability has been obtained by merging different information: (a) the maximal probability should be found for a closing crack, (b) the probability should increase far from the pure DC model and (c) the probability should decrease from expected negative isotropic sources to positive isotropic sources. Note that the sign of the isotropic component is safely derived because the decomposition of the MT into isotropic and deviatoric components is unique. However, the sign and size of the CLVD term can be different depending on the chosen decomposition, e.g. expressing the source as the superposition of a closing crack and a different deviatoric term. Consistent negative CLVD and isotropic components are found if the collapse part of the event radiates most of the seismic energy. An example of different possible decompositions is discussed in the following section, for the case of the 1996

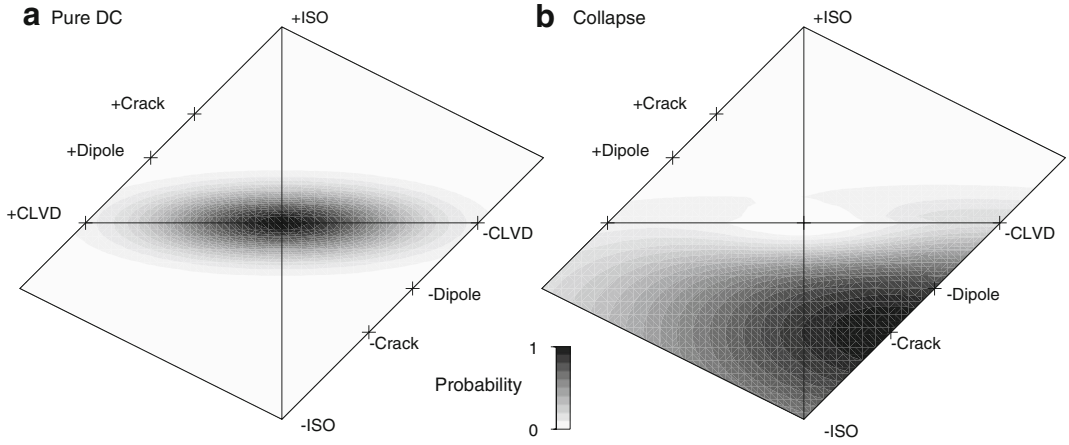

Fig. 6 Chosen prior probabilities (according to the colour scale plotted at the bottom) are shown using source type plots for different rupture processes: **a** pure DC; **b** collapse

Teutschenthal earthquake. Results of the Bayesian analysis are summarised in Fig. 7 for all 30 events. Results confirm previous findings, showing that the collapse scenario is preferred only for the Teuschenthal and Völkershausen events.

6 The 1996 Teutschenthal and 1989 Völkershausen induced earthquakes

On 11 September 1996, at 3:36:35 UT, a M_L 4.8 earthquake struck the Teutschenthal potash mine, near Halle, Germany. The epicentral location, according to the BGR catalogue was 51.44 latitude N 11.84 longitude E. The depth of the event can be fixed at 700 m, known depth of excavations. Mining was performed for several decades in this region, and a similar event (M_L 4.3) occurred in 1940 in the same mine, causing 42 casualties within miners. However, the mine was out of production since 2 years at the moment of the collapse, and no human activity was reported shortly before the event occurrence (Krüger and Klinge 2002). Local observation indicated the seismic event was due to carnallite pillars breakage and roof collapse. A maximal vertical coseismic subsidence of about 45 cm was observed at the surface. Seismological observations at regional distances have been discussed by Krüger and Klinge (2002), providing a detailed analysis of available data and valuable reference estimations for parameters such as the energy release (7×10^{15} Nm, M_w 4.5) and the rupture area (2.7 km^2). Several broadband stations (Fig. 8) from the GRSN and temporal network recorded the event throughout all Germany, five of them (CLL, CLZ MOX, BRNL and T9BG) were located at less than 200 km and provide an optimal azimuthal coverage of the epicentre. All stations where P onset polarities could be picked indicate negative onsets. This radiation pattern is consistent with implosive source, pillar bursts and a vertical closure of the mining cavities. Signals at the five closest stations show multiple (negative) P onsets, which are most likely the result of multiple sub-events. Krüger and Klinge (2002) identified three main onsets and associate them to three sub-events, the first one releasing less energy, than the others. The differential delay of the second and third pulses at different stations were used to infer a rupture directivity, which would propagate roughly from SW to NE. Surface waves are also strongly excited, given the very shallow source depth. The spectral composition of surface waves shows a different pattern, depending on the station azimuth: low frequencies are observed toward SE at stations MOX and CLL, while high frequencies and scattering are observed toward North (CLZ, T9BG and BRNL). Teyssoneyre et al. (2002) derived the temporal evolution of the moment tensor by inverting bodywave (P) waveforms in the time domain. The authors identified two sub-events: the first characterised by a strong explosive isotropic component and the second consisting of an almost pure DC with strike–slip focal mechanism. These mechanisms do not fit the expected rupture process and the observations, including the first onset polarities.

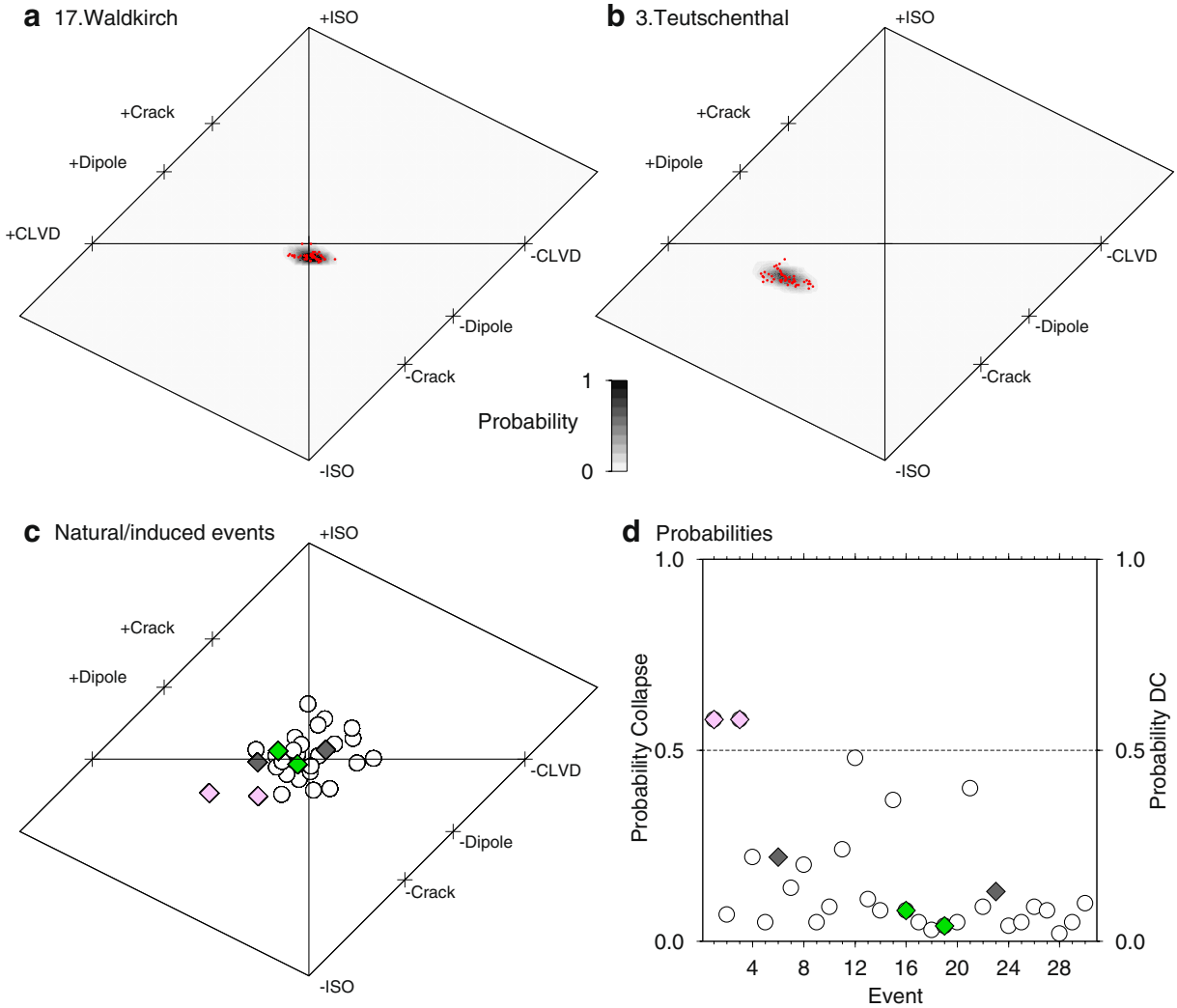

Fig. 7 Source type diagrams after different steps of the discrimination approach. (**a**, **b**) Jackknife results (results of single inversions are denoted by *red points*, the derived probability density function as *grey scale*) for a natural (Waldkirch) and an induced (Teutschenthal) event. **c** Average results for all events, following the jackknife test; different symbols are used to denote induced (*diamond*) and natural (*circle*) seismicity, according to the legend in Fig. 3. **d** Probabilities for the collapse and pure DC scenarios for all events

Following our inversion approach, we first derive the best DC model, presenting a predominant strike–slip rupture. The model reasonably fits amplitude spectra (misfit 0.481) but does not fit waveform phases, specifically at stations CLL and CLZ (Fig. 8a). The misfit of waveforms in the time domain is equal to 0.766. The following full moment tensor inversion leads to a considerably different image of the rupture process, which has a very dominant non-DC part (65 %). This parameter is quite stably retrieved, as shown by minor uncertainties estimations. The confidence interval for the non-DC percentage is 57–73 %, well above percentages obtained for the natural seismicity data set. The full MT model (Fig. 8b) shows a significant improvement of misfit both in the frequency (0.408) and time domain (0.664), with respect to the DC model. The focal mechanism is composed by an implosive isotropic component (23 %), an almost vertical CLVD (42 %), slightly dipping toward NW and a thrust DC mechanism (35 %), with fault planes oriented SW–NE. The scalar moment, which represents the overall release of seismic energy, is equal to 9.86e15 Nm (M_w 4.6). A very shallow centroid

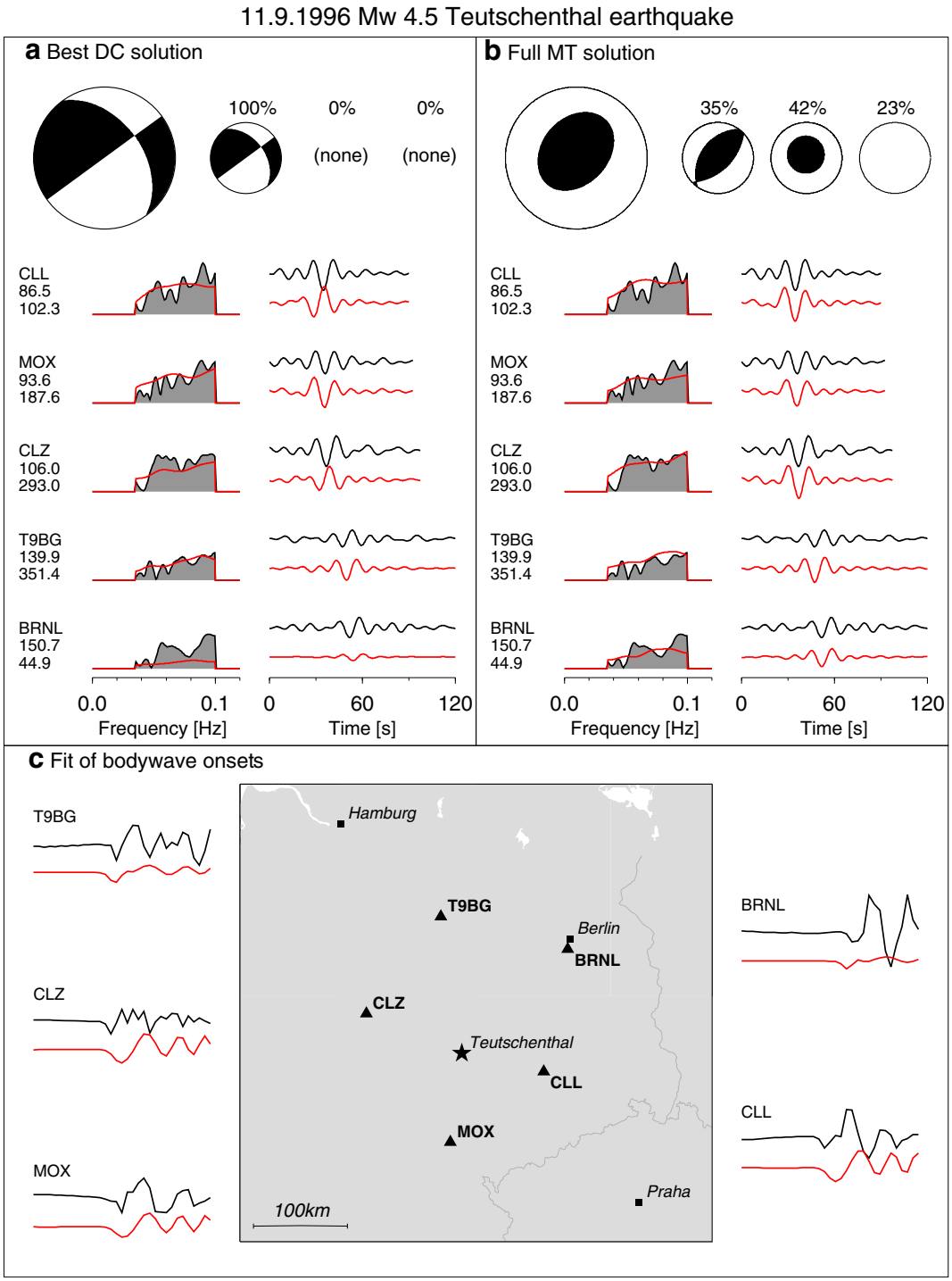

Fig. 8 Moment tensor inversion results for the 11 September 1996 Teutschenthal earthquake. **a** Best DC model and fit of amplitude spectra and 0.035–0.010 Hz filtered displacements (shown for the *vertical component*s of the five closest stations; data are in *black*, synthetics in *red*). **b** Best MT model and its decomposition into DC, CLVD and isotropic terms, and fit of amplitude spectra and 0.035–0.010 Hz filtered displacements. **c** Source location (*star*), closest stations (*triangles*) and first part of the vertical displacements (time windows have a length of 16 s), showing how negative first motions are correctly predicted by our preferred full MT model (*black lines* are observed data, *red lines* are synthetics)

depth (1 km) is correctly derived. Our moment tensor solution is consistent with depicted observations and satisfactorily reproduces first onset polarities (Fig. 7c) at all stations. The implosive isotropic component agrees with the prediction for a physical model of a crack closure, but the CLVD sign does not. As discussed before, while the implosive isotropic component is uniquely derived, an alternative decomposition could be chosen for the deviatoric term. For example, it is possible to decompose the Teutschenthal MT source into a horizontal closing crack (negative isotropic plus negative vertical CLVD) and a deviatoric term, which is the superposition of a NE–SW striking normal fault and a positive CLVD with NW–SE-oriented tension axis. A non-negligible DC component with similar striking is observed, under both decompositions. This DC term is needed to reproduce non-negligible observed Love waves. One possible interpretation for the DC component is the presence of a shear failure accompanying the non-DC process. This hypothesis is supported by the consistency between the orientation of the DC mechanism (NE–SW) and the independent observation of rupture directivity by Krüger and Klinge (2002).

The Völkershausen earthquake occurred on 13 March 1989, at 13:02:16UT at 50.80 N and 10.05 E, in Thuringia, Germany (BGR catalogue). The induced earthquake was the result of bursts of carnallite pillars and subsequent collapse within a potash mine located in the Werra mining area. The rock burst took place at a depth of about 830 m and involved an area of 6.8 km^2, leading to a surface coseismic displacement of about 80 cm (Leydecker et al. 1998; the differential subsidence was estimated after 18 h). Macroseismic data (Leydecker et al. 1989) indicates an elliptical rupture area, mostly elongated along a North–South direction. According to Ahorner (1998), several seismic stations, at local and regional distances in Germany, recorded negative first onsets. Waveforms indicated a complex rupture process which occurred in a few seconds. Several negative pulses suggest different sub-events with similar mechanisms. The available information on the seismic source concerns its depth (900±200 m), local magnitude (M_L 5.6) and epicentral location (Ahorner 1998); no moment tensor inversions were performed so far. The availability of broadband stations in 1989 was limited, and only five stations (11 traces) could be used for the inversion. The network is strongly asymmetric, with most of stations (Gräfenberg array) located towards SE. Results indicate a full MT focal mechanism partially similar to the one obtained for the Teutschenthal event. The full MT solution can be decomposed into 34 % implosive isotropic component, a 18 % oblique CLVD (the sub-vertical dipole dipping toward ENE) and a 48 % thrust DC term. With this mechanism, we can well fit the data and reproduce negative first motion polarities at almost all stations used for the moment tensor inversion. The oblique dipping of the CLVD term is different from the result obtained for the Teutschenthal event, and it is hardly interpreted within a collapse rupture model. This result could be an artefact due to the strong network asymmetry and lack of data. On the other hand, the orientation of the deviatoric component (DC and CLVD) is consistent with the North–South rupture extension, which arises from the macroseismic analysis. We correctly estimate a very shallow source and also obtain the first scalar moment estimation (4.14e16Nm, M_w 4.9) for this event, which is the largest induced event ever recorded in the region.

7 Conclusions

The potential of full moment tensor inversion and decomposition to discriminate natural and induced seismicity has been investigated in this work, choosing a data set of natural and induced seismicity in central Europe as a case study. Results show that large, significant non-double couple components characterise the seismic sources of certain induced events and may be detected by full waveform moment tensor inversion tools. Significant non-double couple components are found whenever a relevant part of the seismic energy is released by processes such as cavity collapses and pillar bursts. In our approach, we have highlighted the limitations of a waveform inversion approach for a stable estimation of non-DC components. We propose the adoption of a common approach, in which the chosen natural and induced seismicity have shallow depths, a similar range of magnitudes and where the moment tensor inversion is carried out using a robust station configurations and inversion algorithms. The analysis of full moment tensor inversion results, which includes uncertainty estimation and the use of several indicators, can then be applied to detect specific induced events. In favourable conditions, events associated to collapse, pillar bursts and blasts may be recognised, whereas other

induced events, characterised by shear fracturing cannot be distinguished with this approach. Two induced events, associated to pillar bursts and roof collapse in potash mines, namely at Völkershausen and Teutschenthal, are identified as induced events. Two more events following coal mining show suspicious non-DC terms but cannot be safely identified as induced ones. Gas exploitation induced seismicity are well described by DC models. Inversion results confirm that induced seismicity in the region plays a relevant role, having moment magnitudes comparable to those of natural seismicity. From the determination of scalar moments and moment magnitudes, we can assert that induced earthquakes in this area are limited to moderate magnitudes never exceeding, so far, M_w 5.0. Inversions results point out that the two most significant induced events, the M_w 4.6 Teutschenthal (11 September 1996) and the M_w 4.9 Völkershausen (13 March 1989) events, occurred as consequence of pillar bursts and roof collapses. These rupture models can reproduce other complementary observations, such as the detection of negative first onsets at all azimuths or the general pattern of surface subsidence. We propose the adoption of a Bayesian approach to evaluate the likelihood of different scenarios for a given earthquake. Results from future applications of this method can improve and redefine the prior probabilities used as input to the Bayesian scheme. Future development of our approach should explore the possibility of combining source location, source depth, non-DC terms and frequency–magnitude distributions in a common discrimination framework. Our results suggest that source depth could be a possible discriminant, although depth resolution is currently limited in our approach.

Acknowledgments We thank two anonymous reviewers, Dr. B. Dost, and Dr. L. Passarelli, and Dr. F. Krüger for valuable suggestions and S. Monna for revising the English text. We acknowledge the BGR and Dr. K. Stammler for providing fast and automated access to processed waveforms from German networks. The facilities of BGR, GEOFON and ORFEUS were used for accessing parts of the waveform and metadata required in this study. We acknowledge all institutions providing seismic data used in this research: GRSN (including stations from Bayern and Saxon seismic network), GEOFON, GEOSCOPE, MEDNET, Swiss Seismological Network, Czech Seismic Network, Austrian Seismic Network and GFZ project TOR. Figures were produced using GMT (Wessel and Smith 1998) and MoPaD (Krieger and Heimann 2012). This work has been funded by the project MINE. The project MINE is part of the R&D Programme GEOTECHNOLOGIEN. The MINE project is funded by the German Ministry of Education and Research (BMBF), grant of project BMBF03G0737.

References

Ahorner L (1998) Entstehung und Ablauf des Gebirgsschlages von Völkershausen am 13. März 1989 in Kalibergbaugebiet des Werratals, Thüringen, aus seismologischer Sicht. Geol Jahrb E 55:25–46

Aki K, Richards PG (1980) Quantitative seismology. Freeman and Co., New York

Bernardi F, Braunmiller J, Kradolfer U, Giardini D (2004) Automatic regional moment tensor inversion in the European–Mediterranean region. Geophys J Int 157:703–716

Braunmiller J, Kradolfer U, Baer M, Giardini D (2002) Regional moment tensor determination in the European–Mediterranean area—initial results. Tectonophysics 356:5–22

Braunmiller J, Dahm T, Bonjer KP (2007) Source mechanism of the 1992 Roermond earthquake from surface-wave inversion of regional data. Geophys J Int 116:663–672

Buforn E, Pro C, Cesca S, Udias A, del Fresno C (2011) The 2010 Granada, Spain, deep earthquake. Bull Seismol Soc Am 101(5):2418–2430

Cesca S, Buforn E, Dahm T (2006) Moment tensor inversion of shallow earthquakes in Spain. Geophys J Int. doi:10.1111/j.1365-246X.2006.03073.x

Cesca S, Heimann S, Stammler K, Dahm T (2010) Automated procedure for point and kinematic source inversion at regional distances. J Geophys Res. doi:10.1029/2009JB006450

Cesca S, Dahm T, Juretzek C, Kühn D (2012) Rupture process of the 7 May 2001 M_w 4.2 Ekofisk induced earthquake. Geophys J Int. doi:10.1111/j.1365-246X.2011.05151.x

Custodio S, Cesca S, Heimann S (2012) Fast kinematic waveform inversion and robustness analysis: application to the 2007 M_w 5.9 Horseshoe Abyssal Plain, offshore SW Iberia, earthquake. Bull Seismol Soc Am 102(1):361–376

Dahm T, Kruger F, Stammler K, Klinge K, Kind R, Wylegalla K, Grasso JR (2007) The 2004 M_w 4.4 Rotenburg, Northern Germany, earthquake and its possible relationship with gas recovery. Bull Seismol Soc Am 97:691–704

Deichmann D (2011) Earthquakes in Switzerland and surrounding regions 1996–2010. Version 2011.1 Swiss Sweismological Service-ETH Zürich, 176pp

Dreger SD, Ford SR, Walter WR (2008) Source analysis of the Crandall Canyon, Utah, mine collapse. Science 321:217

Dziewonski AM, Chou TA, Woodhouse JH (1981) Determination of earthquake source parameters from waveform data for studies of global and regional seismicity. J Geophys Res 86:2825–2852

Fischer T, Horálek J, Michálek J, Boušková A (2010) The 2008 West Bohemia earthquake swarm in the light of the WEBNET network. J Seismol. doi:10.1007/s10950-010-9189-4

Ford SR, Dreger DS, Walter WR (2009) Identifying isotropic events using a regional moment tensor inversion. J Geophys Res 114:B01306. doi:10.1029/2008JB005743

Gilbert (1970) Excitation of the normal modes of the earth by earthquake sources. Geophys J R Astron Soc 22:223–226

Hasegawa HS, Wetmiller RJ, Gendzwill DJ (1989) Induced seismicity in mines in Canada—an overview. Pure Appl Geophys. doi:10.1007/BF00874518

Heimann S (2011) A robust method to estimate kinematic earthquake source parameters. PhD Thesis, University of Hamburg, Hamburg, Germany

Hudson JA, Pearce RG, Rogers RM (1989) Source Type plot for inversion of the moment tensor. J Geophys Res 94(B1):765–774

Jost ML, Hermann RB (1989) A student's guide to and review of moment tensors. Seismol Res Lett 60:37–57

Julian BR, Miller AD, Foulger GR (1998) Non-double-couple earthquakes 1. Theory. Rev Geophys 36:4. doi:10.1029/98RG00716

Kass RE, Raftery AE (1995) Bayes Factors. J Am Stat Assoc 90:773–795. doi:10.2307/2291091

Krieger L, Heimann S (2012) *MoPaD*—moment tensor plotting and decomposition: A tool for graphical and numerical analysis of seismic moment tensors. Seismol Res Lett 83(3):589–595

Krüger F, Klinge K (2002) The 1996 Teutschenthal potash mine collapse: an unusual event with an unusual mechanism. In: Korn M (eds) Ten years of German seismic network (GRSN), Senate Commission for Geosciences, Report 25. Wiley-VCH, Weinheim

Leydecker G (1998) Beziehung zwischen Magnitude und Groesse des Bruchfeldes bei starken Gebirgsschlaegen im deutschen Kalibergbau - ein Beitrag zur Gefaehrdungsprognose. Z angew Geol 44, 1:22–25

Leydecker G, Grünthal G, Ahorner L (1998) Der Gebirgsschlag vom 13. März 1989 bei Völkershausen in Thüringen im Kalibergbaugebiet des Werratals—Makroseismische Beobachtungen und Analysen. Geol Jahrb E 55:5–24

Miller AD, Foulger GR, Julian BR (1998) Non-double-couple earthquakes 2. Observations. Rev Geophys 36:4. doi:10.1029/98RG00717

Minson SE, Dreger DS (2008) Stable inversion for complete moment tensors. Geophys J Int 174. doi:10.1111/j.1365-246X.2008.03797.x

Ottemöller L, Nielsen HH, Atakan K, Braunmiller J, Haskov J (2005) The 7 May 2001 induced seismic event in the Ekofisk oil field, North Sea. J Geophys Res 100. doi:10.1029/2004JB003374

Passarelli L, Maccaferri F, Rivalta E, Dahm T, Boku EA (2011) A probabilistic approach for the classification of earthquakes as 'triggered' or 'not triggered'. J Seismol, submitted

Pondrelli S, Morelli A, Ekström G, Mazza S, Boschi E, Dziewonski AM (2002) European–Mediterranean regional centroid-moment tensors: 1997–2000. Phys Earth Planet Inter 130:71–101

Pondrelli S, Morelli A, Ekström G (2004) European-Mediterranean regional centroid-moment tensor catalog: solutions for years 2001 and 2002. Phys Earth Planet Inter 145(1–4):127–147

Pondrelli S, Salimbeni S, Morelli A, Ekström G, Boschi E (2007) European–Mediterranean regional centroid moment tensor catalog: solutions for years 2003 and 2004. Phys Earth Planet Inter 164(1–2):90–112

Rohr A (2011) Moment tensor inversion of induced earthquakes in Germany, Diploma Thesis, Univ. Hamburg, Germany, 138pp

Šílený J, Milev A (2008) Source mechanism of mining induced seismic events—resolution of double couple and non double couple models. Tectonophysics 456:3–15

Simpson DW, Leith W (1985) The 1976 and 1984 Gazli, USSR, earthquakes—were they induced? Bull Seismol Soc Am 75 (5):1465–1468

Teyssoneyre V, Feignier B, Šílený J, Coutant O (2002) Moment tensor inversion of regional phases: application to a mine collapse. Pure Appl Geophys 159:111–130

Vavrycuk V (2001) Inversion for parameters of tensile earthquakes. J Geophys Res 106(B8):16.339–16.355

Wang R (1999) A simple orthonormalization method for stable and efficient computation of Green's functions. Bull Seismol Soc Am 89(3):733–741

Wessel P, Smith WHF (1998) New improved version of the generic mapping tools released. Eos Trans. AGU 79, p. 579